Size Effects and Temperature Dependence in the Thermal Conductivity of γ-Ga_2O_3 Films

Seungwon Park,[1] Yuxing Liang,[1] Jingyu Tang,[2] Kunyao Jiang,[2] Abhishek Pathak,[1] Robert F. Davis,[2] Lisa M. Porter,[2] and Jonathan A. Malen[2]
[1)]*Department of Mechanical Engineering, Carnegie Mellon University, Pittsburgh, Pennsylvania 15213, USA*
[2)]*Department of Materials Science and Engineering, Carnegie Mellon University, Pittsburgh, Pennsylvania 15213, USA*

(*Electronic mail: jonmalen@andrew.cmu.edu)

(Dated: 27 May 2025)

The thermal conductivities of (100) γ-Ga_2O_3 films deposited on (100) $MgAl_2O_4$ substrates with various thicknesses were measured using frequency-domain thermoreflectance (FDTR). The measured thermal conductivities of γ-Ga_2O_3 films are lower than the thermal conductivities of $(\bar{2}01)$ β-Ga_2O_3 films of comparable thickness, which suggests that γ-phase inclusions in the doped or alloyed β-phase may affect its thermal conductivity. The thermal conductivity of γ-Ga_2O_3 increases from $2.3^{+0.9}_{-0.5}$ W/m·K to 3.5 ± 0.7 W/m·K for films with thicknesses of 75 nm to 404 nm, which demonstrates a prominent size effect on thermal conductivity. The thermal conductivity of γ-Ga_2O_3 also shows a slight increase as temperature increases from 293 K to 400 K. This increase in thermal conductivity occurs when defect and boundary scattering suppress signatures of temperature-dependent Umklapp scattering. γ-Ga_2O_3 has a cation-defective spinel structure with at least two gallium vacancies in every unit cell, which are the likely source of defect scattering.

Gamma-gallium oxide (γ-Ga_2O_3) has attracted significant interest due to its intrinsic defects and its frequent appearance as a secondary phase during the synthesis of β-Ga_2O_3 thin films. Unlike the thermodynamically stable β-Ga_2O_3 phase, γ-Ga_2O_3 adopts a defective spinel crystal structure, which intrinsically contains local distortions and disorder due to the coexistence of tetrahedral and octahedral gallium sites.[1–7] Despite its defect structure, γ-Ga_2O_3 exhibits distinct electronic and optical properties, including tunable photoluminescence[8–10] and varying bandgaps,[11,12] which position it as a promising material for emerging optoelectronics applications. Additionally, its open structure offers ample sites for active catalytic activities,[13] highlighting its potential for methanol steam reforming[14] and photocatalytic degradation of volatile organic compounds.[15] γ-Ga_2O_3 frequently forms as unintended inclusions during the synthesis of doped or alloyed β-Ga_2O_3 films and nanostructures under non-equilibrium growth conditions such as pulsed laser deposition (PLD),[16,17] chemical vapor deposition (CVD),[5–7,18] and plasma-assisted molecular beam epitaxy (PAMBE).[19]

The inclusion of γ-Ga_2O_3 in β-Ga_2O_3 thin films has raised concerns regarding thermal management in high-power electronic devices. β-Ga_2O_3, with its ultrawide bandgap ($\sim$4.8 eV) and high breakdown electric field strength (8 MV/cm),[20] has been widely studied as a next-generation semiconductor material for power electronics and deep-ultraviolet photodetectors. However, β-Ga_2O_3 has a low thermal conductivity (11–27 W/m·K)[21] compared to other wide bandgap semiconductors such as GaN (210 W/m·K) and 4H-SiC (270 W/m·K),[22] which poses a significant challenge for efficient heat dissipation in devices. Given the frequent occurrence of γ-Ga_2O_3 in β-Ga_2O_3 films, understanding the thermal behavior of the γ-phase is crucial for accurately predicting and optimizing β-Ga_2O_3-based electronic device performance. Moreover, γ-Ga_2O_3's potential for catalytic applications further underscores the need for detailed investigations of its thermal transport properties, as thermal conductivity governs the self-cooling (heating) of endothermic (exothermic) catalytic reactions.[23,24]

While the thermal properties of β-Ga_2O_3 have been extensively studied, those of γ-Ga_2O_3 remain largely unexplored. Single-crystal β-Ga_2O_3 exhibits anisotropic thermal conductivity with reported values of 27.0 ± 2.0 W/m·K along the [010] direction and 10.9 ± 1.0 W/m·K along the [100] direction.[21] Thin films of β-Ga_2O_3 show a reduced thermal conductivity compared to bulk materials as phonon boundary scattering dominates Umklapp scattering for sub-micron thicknesses. For example, the thermal conductivity in β-Ga_2O_3 thin films has been observed to increase progressively from 6.3 ± 0.6 W/m·K to 10.8 ± 1.2 W/m·K with thickness increasing from 164 nm to 2500 nm.[25] This suggests that phonons with mean free paths (MFPs) greater than 1 μm contribute to the thermal conductivity of β-Ga_2O_3.

In this study, systematic measurements were conducted on γ-Ga_2O_3 films with different thicknesses across a temperature range of 293 K to 400 K to reveal thermal transport properties of γ-Ga_2O_3 and the size effects in the films. The results are compared with β-Ga_2O_3 thermal conductivity values from the literature and with results from measurements taken using the same experimental setup to highlight the difference in heat transfer mechanisms between the two phases. This work provides experimental measurements of thermal conductivity for γ-Ga_2O_3 films, which is essential for both mitigating its impact in β-Ga_2O_3-based devices and leveraging its potential in independent applications.

Five γ-Ga_2O_3 films with thicknesses ranging from 70 to 404 nm were grown on (100) $MgAl_2O_4$ (spinel) substrates at 743 K.[7] Additionally, two β-Ga_2O_3 films with thickness of 175 nm and 355 nm were grown on (0001) Al_2O_3 (c-plane sapphire) substrates at 1073 K enabling a direct comparison of the thermal conductivity between these two polymorphs. All seven films were grown using a vertical, low-

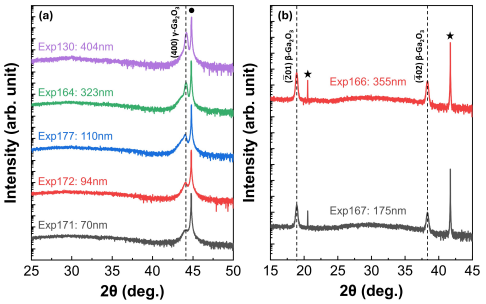

FIG. 1: **Room-temperature XRD 2θ-ω scans for the (a) five γ-Ga_2O_3 films on (100) spinel and (b) two β-Ga_2O_3 films on c-plane sapphire. The black circle and star symbols represent reflections from the corresponding substrates.**

pressure, cold-wall metal-organic chemical vapor deposition reactor. Detailed growth parameters are provided in Table I. Triethylgallium (TEGa) and O_2 were used as the reactants, with N_2 serving as the carrier gas for the TEGa precursor. The O/Ga (VI/III) ratios were maintained at 635 and 3364 for the growth of γ-Ga_2O_3 and β-Ga_2O_3, respectively. High-resolution X-ray diffraction (HR-XRD) and X-ray reflectivity (XRR) measurements were acquired using a PANalytical X'Pert Pro MPD X-ray diffractometer for phase identification and thickness determination.

Figure 1(a) shows the out-of-plane 2θ-ω scans of the five γ-Ga_2O_3 films grown on a (100) spinel substrate. The peaks located at 44.14° and 44.82° are attributed to (400) γ-Ga_2O_3 and (400) spinel, indicating that the γ-Ga_2O_3 films were epitaxially stabilized on spinel substrate, as they share the same crystal structure with an approximate lattice mismatch of +1.9%. The intensity of the (400) γ-Ga_2O_3 peak increases with the film thickness, as thicker films provide more diffraction planes. Figure 1(b) shows the out-of-plane 2θ-ω scans of the two β-Ga_2O_3 films grown on c-plane sapphire. Two peaks located at 18.91° and 38.33° are attributed to $(\bar{2}01)$ and $(\bar{4}02)$ β-Ga_2O_3, respectively. No other peaks, aside from the (0003) (2θ = 20.53°) and (0006) (2θ = 41.72°) sapphire substrate peaks, were observed, indicating that the β-Ga_2O_3 films were highly $(\bar{2}01)$ oriented. This orientation of β-Ga_2O_3 has a similar oxygen atomic arrangement as the (0001) plane of sapphire.

TABLE I: **Summary of the growth parameters of the seven Ga_2O_3 films ($5\gamma + 2\beta$) investigated in this study.**

Exp. No.	Substrate	Growth temperature (°C)	Reactor pressure (Torr)	TEGa molar flow rate (mole/min)	O_2 molar flow rate (mole/min)	O/Ga (VI/III) ratio	Growth period (min)	Film thickness (nm)	Observed phase
Exp. 130	(100) spinel	470	20	7.02×10^{-5}	2.23×10^{-2}	635	60	404	γ
Exp. 164	(100) spinel	470	20	7.02×10^{-5}	2.23×10^{-2}	635	40	323	γ
Exp. 177	(100) spinel	470	20	7.02×10^{-5}	2.23×10^{-2}	635	17	110	γ
Exp. 172	(100) spinel	470	20	7.02×10^{-5}	2.23×10^{-2}	635	12	94	γ
Exp. 171	(100) spinel	470	20	7.02×10^{-5}	2.23×10^{-2}	635	7	70	γ
Exp. 166	(0001) sapphire	800	20	1.33×10^{-5}	2.23×10^{-2}	3364	90	355	β
Exp. 167	(0001) sapphire	800	20	1.33×10^{-5}	2.23×10^{-2}	3364	45	175	β

A 5 nm adhesion layer of Cr capped with an 80 nm Au transducer layer was deposited on top of Ga_2O_3 films using a Kurt Lesker PVD 75 Electron Beam Evaporator for thermal conductivity measurements. The Cr layer provides strong adhesion between the Au transducer and the film, which enhances the thermal boundary conductance.[26] The true thicknesses of the Au transducer and Cr adhesion layer were measured using XRR. The composite electrical conductivity of the Au/Cr transducer was measured with the four-point probe (4PP) method. The Wiedemann-Franz law was used to determine the Au/Cr thermal conductivity from the electrical conductivity.

The thermal conductivity of γ-Ga_2O_3 was measured using frequency domain thermoreflectance (FDTR). FDTR is a non-contact optical technique where continuous wave pump and probe lasers are used to heat a sample and measure its thermal response. The pump laser beam (488 nm) is intensity-modulated by an electro-optic modulator (EOM) with sinusoidal modulation. When focused onto the sample, it acts as a temporally periodic, spatially gaussian heat source. The pump laser is absorbed by the Au transducer thereby inducing a temperature response that exhibits phase lag relative to heating that depends on the thermal properties of the sample. The phase lag is monitored by the co-aligned probe laser beam (532 nm), based on the thermoreflectance of Au, across multiple modulation frequencies. The phase data is fitted with an analytical solution of the heat diffusion equation for periodic heating of a layered solid to extract unknown thermal properties - in this case, the thin film thermal conductivity k.[27]

To minimize uncertainty in the fitted value $k_{\gamma\text{-}Ga_2O_3}$, other input parameters to the analytical model were pre-determined. The thickness of γ-Ga_2O_3, $L_{\gamma\text{-}Ga_2O_3}$, was measured using X-

ray reflectometry (XRR) analysis, with an estimated uncertainty of $\pm 5\%$. The specific heat $c_{\gamma\text{-}Ga_2O_3}$ is 480 ± 5 J/kg·K at 300 K[28] and is converted to the volumetric heat capacity by multiplying with the literature-reported density (5760.7 kg/m^3).[29] The laser spot radius (3.5 ± 0.2 μm) was measured using a reference sample (Au on fused silica), and it was used as a fixed parameter for the fitting algorithm. FDTR was used to measure the thermal conductivity of the spinel substrate (k_{spinel} = 19 ± 3 W/m·K) in advance. The remaining unknown parameters are then $k_{\gamma\text{-}Ga_2O_3}$ and the thermal boundary conductances at the Cr/γ-Ga_2O_3 interface (G_{12}) and the at γ-Ga_2O_3/spinel interface (G_{23}).

To extract $k_{\gamma\text{-}Ga_2O_3}$, G_{12} and G_{23} need to be concurrently fitted, leaving three fitting parameters for each sample, which can lead to high uncertainties. To address this, we implemented a multi-fit iteration algorithm to enable the simultaneous extraction of more than two fitting parameters over multiple samples with reduced uncertainty. The workflow of this iteration algorithm is shown in Fig. 2 (a). The key assumption behind this algorithm is that G_{12} and G_{23} are uniform for all five samples, as the samples were prepared with identical growth and deposition methods. The goal of this algorithm is to find five datasets (one from each sample) with the lowest combined mean-squared error (MSE) of fit relative to phase data when using G_{12} and G_{23} as shared variables.

To start, 25 (5x5 square grid with 10 μm increments) FDTR measurements were performed on each sample, as shown in Fig. 2(b). The algorithm randomly chooses one dataset for each sample. From the five datasets, G_{12} and G_{23} are extracted as shared variables using the non-linear fitting routine. This fitting algorithm finds the values of G_{12} and G_{23} that yield the minimum MSE between the data set and the heat diffusion model. Once G_{12} and G_{23} are extracted, the thermal conductivity and the MSE of the entire 125 datasets (25 measurements x 5 samples) were computed using G_{12} and G_{23} as fixed parameters. From the filtered list, we chose the dataset with the lowest MSE from each sample. With five chosen datasets, we used the non-linear fitting algorithm again to extract new G_{12} and G_{23} as shared variables and new $k_{\gamma\text{-}Ga_2O_3}$ for each dataset. We repeated this routine until the currently chosen datasets matched the previous set and recorded the extracted TBCs and the thermal conductivity of five samples. The Monte Carlo method was used to quantify the uncertainty of the FDTR measurement.[30] Figure 3 shows the experimental thermal conductivity of both γ-Ga_2O_3 and β-Ga_2O_3. The thermal conductivity of γ-Ga_2O_3 increases from $2.3^{+0.9}_{-0.5}$ W/m·K to 3.5 ± 0.7 W/m·K for films varying in thickness from 75 nm to 404 nm. A similar relationship between the thermal conductivity and film thickness was observed for β-Ga_2O_3.

The thermal conductivity of a non-metal where phonons dominate heat transport is defined as

$$k = \frac{1}{3}\int C(\omega)v(\omega)\Lambda(\omega)\,d\omega, \tag{1}$$

where $C(\omega)$ is the volumetric heat capacity at phonon frequency ω [J/m^{3}K], $v(\omega)$ is the average phonon group velocity at phonon frequency ω [m/s], and $\Lambda(\omega)$ is the phonon

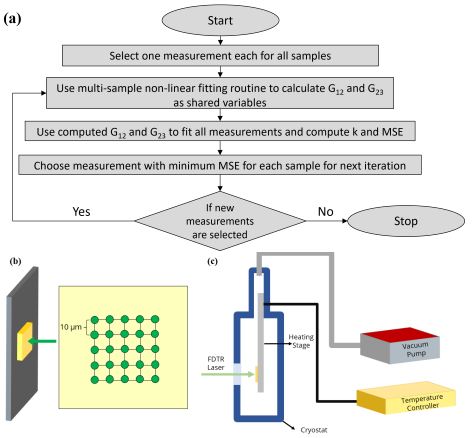

FIG. 2: **(a) Workflow of the multi-fit iteration algorithm. (b) Schematic of a 5x5 square grid FDTR scan. (c) Schematic of temperature-dependent FDTR measurement.**

mean free path (MFP) at phonon frequency ω [m]. The effective phonon MFP at a specific ω can be determined by the Matthiessen rule,

$$\frac{1}{\Lambda(\omega)} = \frac{1}{\Lambda_U(\omega)} + \frac{1}{\Lambda_{imp}(\omega)} + \frac{1}{\Lambda_b}, \tag{2}$$

where $\Lambda_U(\omega)$ is the phonon MFP from phonon-phonon (Umklapp) scattering, $\Lambda_{imp}(\omega)$ is the phonon MFP from impurity (defect) scattering, and Λ_b is the phonon MFP from boundary scattering. Size effects in thermal conductivity occur when Λ_b becomes comparable to or smaller than $\Lambda_U(\omega)$ and $\Lambda_{imp}(\omega)$. Due to the complex unit cell of γ-Ga_2O_3, there are 3 acoustic branches and 117 optical branches in the phonon dispersion based on the conventional unit cell of the spinel structure.[31] We have thus chosen not to use a simple analytical model based only on acoustic phonon modes for quantitative comparison with our data.

$k_{\gamma\text{-}Ga_2O_3}$ was compared to $k_{\beta\text{-}Ga_2O_3}$ from the literature[32] and our own experiments. Szwejkowski *et al.* reports the effective thermal conductivity of β-Ga_2O_3, which includes the intrinsic thermal conductivity of β-Ga_2O_3 and the thermal boundary conductance at the β-Ga_2O_3/GaN interface, as the films in that study were grown on GaN. For our FDTR measurements, we separated the thermal boundary conductances from the thermal conductivity, so we report the intrinsic thermal conductivity of both β-Ga_2O_3 and γ-Ga_2O_3 films. Our measurements indicate that γ-Ga_2O_3 has a lower thermal conductivity than β-Ga_2O_3 at comparable thickness. Cr/γ-Ga_2O_3 thermal boundary conductance (175^{+109}_{-43} MW/m^{2}K) and Cr/β-Ga_2O_3 thermal boundary conductance (168^{+152}_{-52} MW/m^{2}K) are comparable but lower than the literature-reported Cr/β-Ga_2O_3

thermal boundary conductance (451 MW/m^{2}K), which was taken on single crystal β-Ga_2O_3.[33] Although the transducer deposition method (electron-beam evaporator) was identical, the transducer in Ref. 31 was deposited at a higher level of vacuum (2×10^{-9} torr vs. 5×10^{-7} torr), which could have contributed to reduced impurities at the interface and higher Cr/β-Ga_2O_3 TBC. Notably, the $k_{\gamma\text{-}Ga_2O_3}$ values are insensitive to the thermal boundary conductance in this range. When Cr/β-Ga_2O_3 TBC from the literature is used as a fixed parameter, $k_{\gamma\text{-}Ga_2O_3}$ changes by approximately 6%. The TBC of the γ-Ga_2O_3/spinel interface has no comparable literature reference. The temperature-dependent thermal conductivity of two γ-Ga_2O_3 films were measured as a function of temperature from 293 K to 400 K. Figure 2(c) shows the schematic of the temperature-dependent FDTR setup. The sample is placed inside an optically accessible cryostat, which was pumped down to a pressure of 1.2×10^{-3} torr. We used a PID temperature controller (Oxford Instruments, ITC 503S) to maintain the desired temperature during the measurement. In order to simplify the data analysis, the thermal conductivity of the Au/Cr layer was assumed to be constant at all measured temperatures,[34] as were the G_{12} and G_{23} values.[35] The extracted thermal conductivities of the γ-Ga_2O_3 films are insensitive to these parameters. Based on the sensitivity contour plot, $k_{\gamma\text{-}Ga_2O_3}$ is relatively insensitive to increasing G_{12} and G_{23} with temperature. A 20% increase in G_{12} and G_{23} increases the extracted $k_{\gamma\text{-}Ga_2O_3}$ by 1.5%.

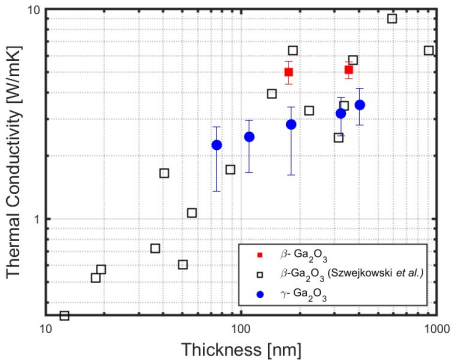

FIG. 3: **Thermal conductivity of β- and γ-Ga_2O_3 as a function of thickness at 293 K.**

Figure 4 shows the temperature-dependent thermal conductivity of γ-Ga_2O_3 from 293 K to 400 K for the samples with thicknesses of 110 nm and 404 nm. In both cases, the thermal conductivity shows a slight increase as temperature rises. This trend deviates from temperature-dependent thermal conductivity of β-Ga_2O_3 films, as shown in our measurement on 175 nm β-Ga_2O_3 and in data from the literature.[21,25] The thermal conductivity of β-Ga_2O_3 monotonically decreases with increasing temperature due to increased Umklapp scattering. As the thickness decreases, the temperature-dependence of the thermal conductivity of β-Ga_2O_3 becomes less prominent, as shown by our measurements of 175 nm β-Ga_2O_3. This is due to increased phonon boundary scattering, where Λ_b is independent of the temperature. In the case of γ-Ga_2O_3, which has a defective spinel structure, we hypothesize that gallium and oxygen vacancies in γ-Ga_2O_3 crystals cause the impurity scattering to be a significant scattering mechanism between 293 K and 400 K. The phonon MFPs set by impurity scattering and boundary scattering are temperature-independent, while heat capacity constantly increases at elevated temperatures. The heat capacity of γ-Ga_2O_3 increases as temperature increases by nearly 10% from 293 K to 400 K.[28] Thus, the temperature-dependence of the thermal conductivity of γ-Ga_2O_3 between 293 K and 400 K is caused by temperature-insensitive phonon scattering with increasing heat capacity. The increase in thermal conductivity with temperature could instead be explained by the contribution of wavelike modes, diffusing via a Zener-like tunneling between quasi-degenerate vibrational eigenstates as can be described by the Wigner Transport Equation.[36] While beyond the scope of this work, low temperature measurements may be able to distinguish the phonon scattering and wavelike tunneling pictures of thermal transport in γ-Ga_2O_3. At higher temperatures, we anticipate that Umklapp scattering will become the dominant scattering mechanism, reducing the average phonon mean free path and potentially causing a decreasing trend in thermal conductivity.

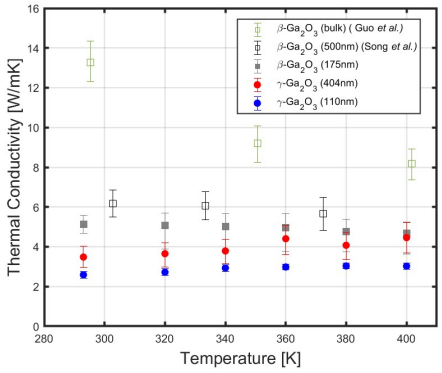

FIG. 4: **Temperature-dependent thermal conductivity of β- and γ-Ga_2O_3 thin films.**

In summary, the thermal conductivities of γ-Ga_2O_3 films were measured using FDTR. We find that the thermal conductivities of γ-Ga_2O_3 films are lower than the thermal conductivities of β-Ga_2O_3 films at comparable thickness. This discrepancy suggests that γ-phase inclusions in doped or alloyed β-phase films could potentially reduce the overall thermal conductivity of the films. γ-Ga_2O_3 shows a similar size dependence as β-Ga_2O_3, where the thermal conductivity increases with increasing film thickness. The temperature-dependent thermal conductivity of γ-Ga_2O_3 shows a moder-

ate increase with increasing temperature from 293 K to 400 K. This trend contrasts with that shown in β-Ga_2O_3, possibly due to temperature-insensitive phonon-defect scattering caused by gallium and oxygen vacancies in the γ-Ga_2O_3 lattice. This work underscores the importance of removing γ-Ga_2O_3 inclusions from β-Ga_2O_3 films for high power applications, as γ-Ga_2O_3's reduced thermal conductivity may impact thermal management and device performance.

Author's Contributions

Seungwon Park: Conceptualization (lead); Data curation (lead); Formal analysis (lead); Methodology (lead); Software (lead); Visualization (lead); Formal analysis (lead); Validation (lead); Writing - original draft (lead); Writing - review & editing (lead). **Yuxing Liang**: Conceptualization (equal); Data curation (equal); Formal analysis (equal); Methodology (equal); Software (equal); Visualization (equal); Formal analysis (equal); Validation (equal); Writing - original draft (equal); Writing - review & editing (equal). **Jingyu Tang**: Conceptualization (equal); Data curation (equal); Formal analysis (equal); Visualization (equal); Writing - original draft (equal); Writing - review & editing (equal). **Kunyao Jiang**: Conceptualization (equal); Data curation (equal); Formal analysis (equal); Visualization (equal); Writing - original draft (support); Writing - review & editing (support). **Abhishek Pathak**: Methodology (equal); Software (equal); Writing - review & editing (support). **Robert F. Davis**: Funding acquisition (lead); Project administration (lead); Supervision (lead); Writing - review & editing (lead). **Lisa M. Porter**: Funding acquisition (lead); Project administration (lead); Supervision (lead); Writing - review & editing (lead). **Jonathan A. Malen**: Funding acquisition (lead); Project administration (lead); Supervision (lead); Writing - review & editing (lead).

Acknowledgments

This work was supported by Northrop Grumman University Research Program, the Army Research Office through Award No. W911NF2220191, the Air Force Office of Scientific Research through Award No. FA9550-21-1-0360, and National Science Foundation (NSF) under Grant No. DMR-2324375. The authors acknowledge use of the Materials Characterization Facility at Carnegie Mellon University supported by grant MCF-677785.

Conflict of Interest

The authors have no conflicts to disclose.

Data Availability

The data that support the findings of this study are available from the corresponding author upon reasonable request.

[1]H. Hayashi, R. Huang, F. Oba, T. Hirayama, and I. Tanaka, "Site preference of cation vacancies in Mn-doped Ga_2O_3 with defective spinel structure," Applied Physics Letters **101**, 241906 (2012).
[2]M. Mitome, S. Kohiki, T. Nagai, K. Kurashima, K. Kimoto, and Y. Bando, "A Rhombic Dodecahedral Honeycomb Structure with Cation Vacancy Ordering in a γ-Ga_2O_3 Crystal," Crystal Growth & Design **13**, 3577–3581 (2013).
[3]H.-L. Huang, J. M. Johnson, C. Chae, A. Senckowski, M. H. Wong, and J. Hwang, "Atomic scale mechanism of β to γ phase transformation in gallium oxide," Applied Physics Letters **122**, 251602 (2023).
[4]H. Y. Playford, A. C. Hannon, M. G. Tucker, D. M. Dawson, S. E. Ashbrook, R. J. Kastiban, J. Sloan, and R. I. Walton, "Characterization of Structural Disorder in γ-Ga_2O_3," **118**, 16188–16198.
[5]J. Tang, K. Jiang, S. D. House, C. Xu, K. Xiao, L. M. Porter, and R. F. Davis, "Mg and Al-induced phase transformation and stabilization of Ga_2O_3-based γ-phase spinels," Applied Physics Letters **123**, 012103 (2023).
[6]K. Jiang, J. Tang, C. Xu, K. Xiao, R. F. Davis, and L. M. Porter, "Evolution of β-Ga_2O_3 to γ-Ga_2O_3 solid-solution epitaxial films after high-temperature annealing," Journal of Vacuum Science & Technology A **41**, 062702 (2023).
[7]J. Tang, K. Jiang, C. Xu, M. J. Cabral, K. Xiao, L. M. Porter, and R. F. Davis, "Atomic-scale investigation of γ-Ga_2O_3 deposited on $MgAl_2O_4$ and its relationship with β-Ga_2O_3," APL Materials **12**, 011109 (2024).
[8]T. Wang, S. S. Farvid, M. Abulikemu, and P. V. Radovanovic, "Size-Tunable Phosphorescence in Colloidal Metastable γ-Ga_2O_3 Nanocrystals," Journal of the American Chemical Society **132**, 9250–9252 (2010).
[9]Y. Teng, L. X. Song, A. Ponchel, Z. K. Yang, and J. Xia, "Self-Assembled Metastable γ-Ga_2O_3 Nanoflowers with Hexagonal Nanopetals for Solar-Blind Photodetection," Advanced Materials **26**, 6238–6243 (2014).
[10]S. S. Farvid, T. Wang, and P. V. Radovanovic, "Colloidal Gallium Indium Oxide Nanocrystals: A Multifunctional Light-Emitting Phosphor Broadly Tunable by Alloy Composition," Journal of the American Chemical Society **133**, 6711–6719 (2011).
[11]T. Oshima, Y. Kato, M. Oda, T. Hitora, and M. Kasu, "Epitaxial growth of γ-$(Al_xGa_{1-x})_2O_3$ alloy films for band-gap engineering," Applied Physics Express **10**, 051104 (2017).
[12]R. Horie, H. Nishinaka, D. Tahara, and M. Yoshimoto, "Epitaxial growth of γ-$(Al_xGa_{1-x})_2O_3$ alloy thin films on spinel substrates via mist chemical vapor deposition," Journal of Alloys and Compounds **851**, 156927 (2021).
[13]T. Watanabe, Y. Miki, T. Masuda, H. Kanai, S. Hosokawa, K. Wada, and M. Inoue, "Pore structure of β-Ga_2O_3-Al_2O_3 particles prepared by spray pyrolysis," **145**, 131–140.
[14]S. E. Collins, L. E. Briand, L. A. Gambaro, M. A. Baltanás, and A. L. Bonivardi, "Adsorption and Decomposition of Methanol on Gallium Oxide Polymorphs," The Journal of Physical Chemistry C **112**, 14988–15000 (2008).
[15]Y. Hou, L. Wu, X. Wang, Z. Ding, Z. Li, and X. Fu, "Photocatalytic performance of α-, β-, and γ-Ga_2O_3 for the destruction of volatile aromatic pollutants in air," Journal of Catalysis **250**, 12–18 (2007).
[16]H. Hayashi, R. Huang, H. Ikeno, F. Oba, S. Yoshioka, I. Tanaka, and S. Sonoda, "Room temperature ferromagnetism in Mn-doped γ-Ga_2O_3 with spinel structure," Applied Physics Letters **89**, 181903 (2006).
[17]H. Hayashi, R. Huang, F. Oba, T. Hirayama, and I. Tanaka, "Atomistic structure and energetics of interface between Mn-doped γ-Ga_2O_3 and $MgAl_2O_4$," Journal of Materials Science **46**, 4169–4175 (2011).
[18]T. Oshima, T. Nakazono, A. Mukai, and A. Ohtomo, "Epitaxial growth of γ-Ga_2O_3 films by mist chemical vapor deposition," Journal of Crystal Growth **359**, 60–63 (2012).
[19]C. S. Chang, N. Tanen, V. Protasenko, T. J. Asel, S. Mou, H. G. Xing, D. Jena, and D. A. Muller, "γ-phase inclusions as common structural defects in alloyed β-$(Al_xGa_{1-x})_2O_3$ and doped β-Ga_2O_3 films," **9**, 051119.
[20]H. Xue, Q. He, G. Jian, S. Long, T. Pang, and M. Liu, "An Overview of the Ultrawide Bandgap Ga_2O_3 Semiconductor-Based Schottky Barrier Diode for Power Electronics Application," **13**, 290.
[21]Z. Guo, A. Verma, X. Wu, F. Sun, A. Hickman, T. Masui, A. Kuramata, M. Higashiwaki, D. Jena, and T. Luo, "Anisotropic thermal conductivity in single crystal β-gallium oxide," **106**, 111909.
[22]M. Higashiwaki, K. Sasaki, H. Murakami, Y. Kumagai, A. Koukitu, A. Kuramata, T. Masui, and S. Yamakoshi, "Recent progress in Ga_2 O_3 power devices," Semiconductor Science and Technology **31**, 034001 (2016).
[23]R. A. Sehr, "The thermal conductivity of catalyst particles," **9**, 145–152.
[24]J. B. Butt, "Thermal conductivity of porous catalysts," **11**, 106–112.
[25]Y. Song, P. Ranga, Y. Zhang, Z. Feng, H.-L. Huang, M. D. Santia, S. C. Badescu, C. U. Gonzalez-Valle, C. Perez, K. Ferri, R. M. Lavelle, D. W. Snyder, B. A. Klein, J. Deitz, A. G. Baca, J.-P. Maria, B. Ramos-Alvarado, J. Hwang, H. Zhao, X. Wang, S. Krishnamoorthy, B. M. Foley, and S. Choi,

"Thermal Conductivity of β-Phase Ga_2O_3 and $(Al_xGa_1-x)_2O_3$ Heteroepitaxial Thin Films," **13**, 38477–38490.
[26]M. Jeong, J. P. Freedman, H. J. Liang, C.-M. Chow, V. M. Sokalski, J. A. Bain, and J. A. Malen, "Enhancement of Thermal Conductance at Metal-Dielectric Interfaces Using Subnanometer Metal Adhesion Layers," **5**, 014009.
[27]K. T. Regner, D. P. Sellan, Z. Su, C. H. Amon, A. J. McGaughey, and J. A. Malen, "Broadband phonon mean free path contributions to thermal conductivity measured using frequency domain thermoreflectance," **4**, 1640.
[28]M. Zinkevich, F. M. Morales, H. Nitsche, M. Ahrens, M. Rühle, and F. Aldinger, "Microstructural and thermodynamic study of γ-Ga_2O_3," **95**, 756–762.
[29]H. Y. Playford, A. C. Hannon, E. R. Barney, and R. I. Walton, "Structures of Uncharacterised Polymorphs of Gallium Oxide from Total Neutron Diffraction," Chemistry – A European Journal **19**, 2803–2813 (2013).
[30]J. Yang, E. Ziade, and A. J. Schmidt, "Uncertainty analysis of thermoreflectance measurements," **87**, 014901.
[31]J. Ding, Y. Liu, X. Gu, L. Zhang, X. Zhang, X. Chen, W. Liu, Y. Cai, S. Guo, and C. Sun, "Electronic transport and optical properties of five different phases (α, β, ε, δ, and γ) of Ga_2O_3: A first-principles study," Physica B: Condensed Matter **682**, 415888 (2024).
[32]C. J. Szwejkowski, N. C. Creange, K. Sun, A. Giri, B. F. Donovan, C. Constantin, and P. E. Hopkins, "Size effects in the thermal conductivity of gallium oxide (β-Ga_2O_3) films grown via open-atmosphere annealing of gallium nitride," **117**, 084308.
[33]H. T. Aller, X. Yu, A. Wise, R. S. Howell, A. J. Gellman, A. J. H. McGaughey, and J. A. Malen, "Chemical Reactions Impede Thermal Transport Across Metal/β-Ga_2O_3 Interfaces," **19**, 8533–8538.
[34]S. J. Mason, D. J. Wesenberg, A. Hojem, M. Manno, C. Leighton, and B. L. Zink, "Violation of the Wiedemann-Franz law through reduction of thermal conductivity in gold thin films," **4**, 065003.
[35]C. Monachon, L. Weber, and C. Dames, "Thermal Boundary Conductance: A Materials Science Perspective," **46**, 433–463.
[36]M. Simoncelli, N. Marzari, and F. Mauri, "Wigner Formulation of Thermal Transport in Solids," Physical Review X **12**, 041011 (2022).